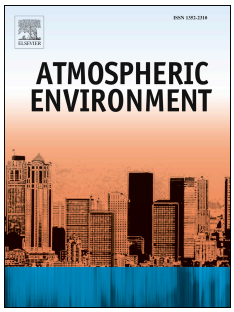

Coal and biomass burning as major emissions of NO_X in Northeast China: Implication from dual isotopes analysis of fine nitrate aerosols

Zhu-Yu Zhao, Fang Cao, Mei-Yi Fan, Wen-Qi Zhang, Xiao-Yao Zhai, Qian Wang, Yan-Lin Zhang

PII: S1352-2310(20)30494-5

DOI: https://doi.org/10.1016/j.atmosenv.2020.117762

Reference: AEA 117762

To appear in: *Atmospheric Environment*

Received Date: 2 March 2020

Revised Date: 9 June 2020

Accepted Date: 6 July 2020

Please cite this article as: Zhao, Z.-Y., Cao, F., Fan, M.-Y., Zhang, W.-Q., Zhai, X.-Y., Wang, Q., Zhang, Y.-L., Coal and biomass burning as major emissions of NO_X in Northeast China: Implication from dual isotopes analysis of fine nitrate aerosols, *Atmospheric Environment* (2020), doi: https://doi.org/10.1016/j.atmosenv.2020.117762.

Graphical Abstract

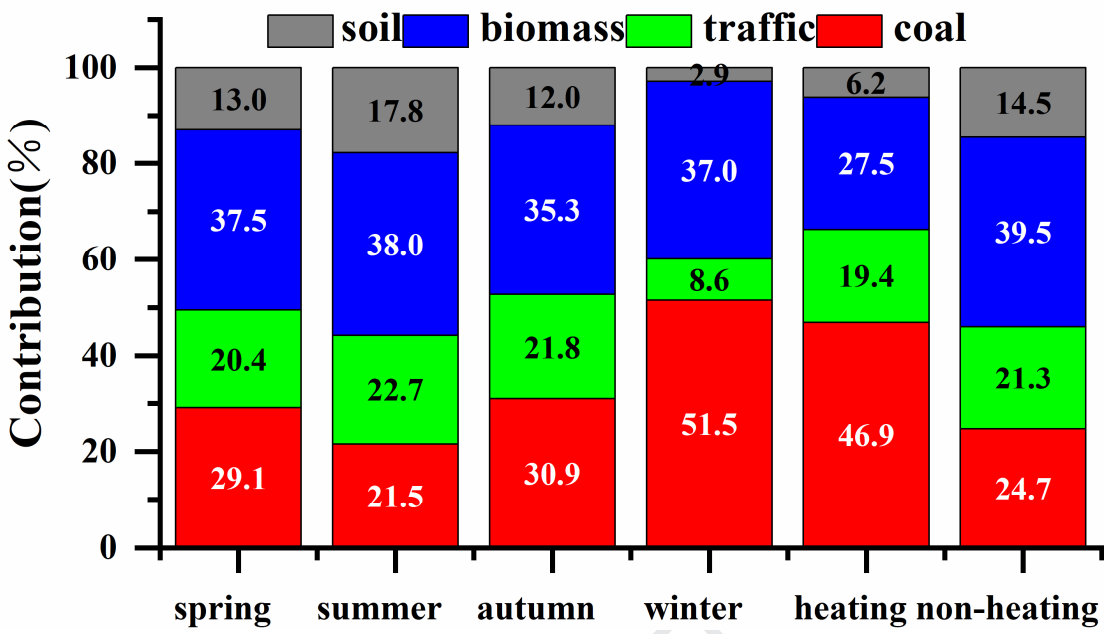

Coal and biomass burning as major emissions of NO_X in Northeast China: implication from dual isotopes analysis of fine nitrate aerosols

Zhu-Yu Zhao [a,b,c], Fang Cao [a,b,c,*], Mei-Yi Fan [a,b,c], Wen-Qi Zhang [a,b,c], Xiao-Yao Zhai [a,b,c], Qian Wang [a,b,c], Yan-Lin Zhang [a,b,c]

[a] *Yale-NUIST Center on Atmospheric Environment, International Joint Laboratory on Climate and Environment Change, Nanjing University of Information Science and Technology, Nanjing, 210044, China.*

[b] *Key Laboratory Meteorological Disaster; Ministry of Education & Collaborative Innovation Center on Forecast and Evaluation of Meteorological Disaster, Nanjing University of Information Science and Technology, Nanjing, 210044, China.*

[c] *Jiangsu Provincial Key Laboratory of Agricultural Meteorology, College of Applied Meteorology, Nanjing University of Information Science & Technology, Nanjing 210044, China.*

Corresponded to Fang Cao (caofangle@163.com)

Abstract

In recent years, there are still huge amounts of NOx emissions in the Northeast, and this inevitably increases the concentration of aerosol nitrate (NO_3^-), which plays an important role in atmospheric pollution. Because of the mixed complicated sources of atmospheric NO_3^-, it is difficult to quantify their contribution, and the use of certain means to identify their sources and pathways is critical to developing effective control measures. Since different sources of NO_X have different ranges of $\delta^{15}N$ values, $\delta^{15}N$ is considered to be a useful tool for identifying the source of aerosol NO_3^-. But isotope

fractionation is produced during the conversion of NO_X to NO_3^-, and $\delta^{18}O$ can be used to estimate its isotope fractionation value. In this study, daily $PM_{2.5}$ samples were collected in four seasons from Northeast China, and their water-soluble ionic components (WSIs), $\delta^{15}N\text{-}NO_3^-$ and $\delta^{18}O\text{-}NO_3^-$ were analyzed. The isotope fractionation value of $\delta^{15}N$ in which NO_X was converted to NO_3^- was estimated and the contribution of different sources was quantified in combination with the Bayesian model. The results showed that NO_3^- was the most important inorganic ion component in the WSIs with the highest annual average ratio of 21.1%. Both $\delta^{15}N$ and $\delta^{18}O$ showed higher in winter ($\delta^{15}N$: 13.79‰±2.17‰; $\delta^{18}O$: 70.50‰±10.02‰) than in summer ($\delta^{15}N$: 2.69‰±2.95‰; $\delta^{18}O$: 58.67‰±4.52‰). The daytime OH· pathway was considered to play a leading role in nitrate formation, with the annual average contribution of 61.0 ±18.8%. NOx was mainly from the contribution of coal combustion (34.5%) and biomass burning (34.3%) followed by traffic (19.5%) and biological soil (11.7%). During heating periods, NOx was dominated by coal combustion with the average contribution of 46.9% whereas biomass burning was the most important contributor during non-heating periods (39.5%). Therefore, controlling coal consumption and biomass burning can drastically reduce concentration of aerosol NO_3^- in Northeast China.

Keywords: Aerosol; Nitrate; Stable isotope; Sources; Formation.

1 Introduction

The secondary inorganic ions, mainly containing sulfate, nitrate and ammonium, are the main components of $PM_{2.5}$ (particulate matter with the aerodynamic diameter less than or equal to 2.5μm) (Shi et al., 2019; Sun et al., 2019; Tian et al., 2016), which play an important role in haze pollution (Chen et al., 2016; Huang et al., 2018; Zhang et al., 2018). In recent years, due to the strict control of sulfur dioxide, the concentration of sulfate in $PM_{2.5}$ is greatly reduced, and the proportion of nitrate is increasing (Xu et al., 2019), especially when pollution events occur during the winter (Feng et al., 2018; Li et al., 2018; Yang et al., 2017). Nitrate in $PM_{2.5}$ is usually produced by oxidation of its gas precursor nitrogen oxides (NOx) (Feng et al., 2018; Pathak et al., 2009; Zhao et al., 2013). NO_X is one of the main pollutants in the atmosphere, and it can exacerbate acid deposition, causing soil acidification and water eutrophication (Boningari and Smirniotis, 2016; Hastings et al., 2013; Skalska et al., 2010). Besides, NO_X plays an important role in tropospheric photochemical reactions (Skalska et al., 2010; Zhao et al., 2013). It affects the production of photochemical smog (Shi et al., 2014) and damages the ozone layer in the stratosphere (Elliott et al., 2019). In recent years, China's economy has developed rapidly, and huge amounts of NO_X emissions have followed (Gu et al., 2013), which have also increased the content of nitrate in aerosols. The NO_X emissions in China were still rising from 2001 (15 ± 3Tg yr^{-1}) to 2015 (22 ± 2Tg yr^{-1}) (Itahashi et al., 2018). The main pathways for atmospheric nitrate formation include the day reaction of droxyl radical (OH·) with NO_2 and the night heterogeneous hydrolysis of N_2O_5 (Boningari and Smirniotis, 2016;

Elliott et al., 2019; Fang et al., 2011; Skalska et al., 2010; Tian et al., 2019). NO_X exists mainly in the atmosphere as NO, during the day, NO is rapidly converted to NO_2 to reach equilibrium, and then react with OH· to produce gaseous nitric acid (HNO_3) (R1-R3, Text S1), which then reacts with ammonia (NH_3) or other alkaline compounds to form nitrate aerosol (Wen et al., 2018a). During the night, the reaction of NO_2 and O_3 produces nitrate radicals (NO_3·), which is in equilibrium with N_2O_5 (R4-R6, Text S1), which can then be adsorbed on the particles to enhance the nitrate aerosol.

The sources of NO_X emissions are divided into natural sources and anthropogenic sources, while natural sources mainly include soil biological (Beyn et al., 2014) and the anthropogenic sources mainly include motor vehicle (traffic), coal combustion and biomass burning emissions (Chen et al., 2019; Elliott et al., 2007; Elliott et al., 2019; Fan et al., 2019). In recent years, stable isotope techniques have been widely used in the analysis of sources of pollutants and are believed to better distinguish between natural and anthropogenic sources of matter (Hastings et al., 2013). The nitrogen isotope $\delta^{15}N$ of atmospheric NO_X is considered to be an important tool for studying its source (He et al., 2018) because that different sources of NO_X have different ranges of $\delta^{15}N$ (Walters et al., 2015b). The $\delta^{15}N$-NOx of coal combustion collected by Felix et al. (Felix et al., 2012) ranged from +9‰ to +26‰. Fibiger and Hastings (Fibiger and Hastings, 2016) first attempted to quantify $\delta^{15}N$-NO_X in biomass burning, which ranged from -7.2‰ to +12‰. The $\delta^{15}N$ value of traffic emissions was -19.1‰ to +9.8‰ (Walters et al., 2015a). Li and Wang (Li and

Wang, 2008) measured the δ^{15}N-NO_X characteristics of soil emissions from -48.9‰ to -19.9‰. Yu and Elliot (Yu and Elliott, 2017) reported that δ^{15}N-NO of soil ranged from -59.8‰ to -23.4‰. Because that N atoms are conserved in the reaction from NO_X to NO_3^- (Wankel et al., 2010), δ^{15}N-NO_3^- is considered to be an important tool for distinguishing nitrates from different NO_X sources, even if there is isotope fractionation in the conversion of NO_X to nitrate. In addition, studies have shown that δ^{18}O have been used to identify pathways for nitrate formation in the atmosphere (Walters and Michalski, 2016; Wang et al., 2019; Wankel et al., 2010; Zong et al., 2018). Generally, δ^{18}O-NO_3^- has a higher value formed by N_2O_5 pathway than by OH· pathway due to that the range of δ^{18}O of atmospheric O_3 is between 90 ‰ and 122 ‰ whereas the δ^{18}O of OH· has an extreme lower range from -25‰ to 0‰ (Hastings, 2004). Therefore, applying the δ^{15}N and δ^{18}O values of atmospheric nitrate can explain its source and formation mechanism.

As an important industrial base in China, Northeast area has serious air pollution problem (Hong et al., 2019). The deterioration of air quality in Northeast China is similar to pollution hotspots such as the Yangtze River Delta and North China Plain (Zhang et al., 2017). Previous research shows that more than 70% of the total NOx emission is derived from coal combustion in China (Chen et al., 2019). Northeast China has very large-scale heating and the heating time is the earliest and longest among all the countries because the especially low temperatures (Hong et al., 2019; Wen et al., 2018b), thus the coal combustion which provides energy for heating will contribute a large amount of NO_X in the Northeast China. Traffic emissions contribute

approximately 20% to global atmospheric NO_X (Anenberg et al., 2017), and this may also be one of the important sources of NO_X in the Northeast. Biomass burning can also produce large amounts of NO_X (Ren et al., 2017) and there are approximately 6Tg NO_X emissions from global biomass combustion each year (Chai et al., 2019). Studies have shown that biomass burning is very important in China (Cao et al., 2017; Chang et al., 2018; Zhang and Cao, 2015), especially in northeastern China where the planting industry is developed and serious agricultural waste burning were occurred during the harvest season (after autumn harvest and before spring tillage) (Cao et al., 2017; Ma et al., 2018). Therefore, the contribution of biomass burning to atmospheric NO_X cannot be ignored in Northeast China. Besides, soil emissions could be a potential source of atmospheric NO_X in northeast China due to its fertile land (Ma et al., 2018). All in all, the source of pollution in the study area is complex and it also complicates the source of atmospheric NO_X in the region. Therefore, study the sources of atmospheric NO_X has a great significance to controlling air pollution in Northeast China.

This is the first attempt to systematically analyze the sources of NO_X in Northeast China. In order to better understand the characteristics of pollution sources in Northeast China, nitrogen and oxygen isotopes of atmospheric NO_X were analyzed and the sources of NO_X was identified in this study. The stable isotope analysis in R (SIAR) model have been applied to quantitatively estimate the contribution of the four potential sources.

2 Materials and methods

2.1 Aerosol sampling collection and atmospheric observations

The campaign was conducted in Chang Chun, an important industrial base in Northeast China, as shown in Figure S1. In 2017, the city's annual average concentration of $PM_{2.5}$ was 46μg.m^{-3} (Li et al., 2019), higher than the National Ambient Air Quality Standards (NAAQS, GB3095-2012) Grade I (35 μg.m^{-3}). It is one of the most densely populated cities in Northeast China and it is an important agricultural base in China.

The daily $PM_{2.5}$ samples of four seasons were collected at Northeast Institute of Geography and Agricultural Ecology, Chinese Academy of Sciences (125.4°N, 44.0°E). The summer, autumn, winter and spring for sampling are defined as May 25 to June 25, 2017, October 10 to November 9, 2017, January 3 to February 1, 2018, and April 3 to May 4, 2018, respectively. The local heating time is from October 25th to April 10th. The heating period during the sampling was defined as October 24 to November 9, 2017, plus January 3 to February 1, 2018 and April 3 to May 4, 2018. The rest of the sampling is the non-heating period.

$PM_{2.5}$ were collected on precombusted (450□ for 6 h) quartz filters (25 × 20 cm) using a high-volume aerosol sampler (KC100, Qingdao, China, at a flow rate of 999L.m^{-3}). After sampling, the film wrapped in aluminum foil was dried in a dry box for 48 hours. Before and after collection, the mass of $PM_{2.5}$ was analyzed using an electronic microbalance (Sartorius BSA124S, Germany,0.1mg) with a ±1 μg precision (at T 25□ and RH 50%±5% during weighing). Then put it in the refrigerator at -20 °C and stored it in a dry box before use.

The data of gas (SO_2, NO_2, O_3) and meteorological elements such as temperature (T), wind speed (WS), relative humidity (RH) and precipitation during the sampling period were derived from China Meteorological Data Network, National Meteorological Information Center. The temperature, wind speed and relative humidity during sampling are shown in Figure S2(a). The concentration of SO_2, NO_2 and O_3 are shown in Figure S2(b).

2.2 Chemical analysis

Each sample was punched once with an 18 mm puncher, dissolved in 15 ml of ultrapure water, and was shaken for 30 minutes using a constant temperature oscillator. Then it was filtered with a 0.22 μm aqueous phase needle filter. Ion chromatography (ICS 5000+, Thermo Fisher Scientific, USA) was used to analyze the daily concentration of WSIs in $PM_{2.5}$, major including NO_3^-, Cl^-, SO_4^{2-}, NH_4^+, Na^+, K^+, $Ca^{2+}$and Mg^{2+}. Details information of ion measurement system and quality control are the same as Fan et al (Fan et al., 2019).

2.3 Isotopic analysis

$\delta^{15}N$ and $\delta^{18}O$ of nitrate were measured using chemical reduction method, details shown in our primary research (Zhao et al., 2019). First, a 18mm filter was punched and dissolved in a certain amount of ultrapure water to make its nitrogen concentration was 0.2ugN/ml. After shaking for 30 min with an ultrasonic shaker, it was filtered with a 0.22 μm aqueous phase needle filter, and 5 ml of the sample solution was stored in a 13 ml centrifuge tube. Then about 1.46 g of sodium chloride was added and pH of the solution was adjusted to 8 by a buffer system formed by 0.5

M hydrochloric acid and 1 M imidazole. Then 0.4-0.5g of cadmium powder (activated by 10% hydrochloric acid) was added to reduce NO_3^- to NO_2^-. The NO_2^- was reduced to N_2O using a sodium azide acetate buffer solution at pH 4.5-4.6, and the $\delta^{15}N$ and $\delta^{18}O$ of N_2O were analyzed by stable isotope ratio mass spectrometer (MAT253, Thermo Fisher Scientific, USA). The $\delta^{15}N$-NO_3^- and $\delta^{18}O$-NO_3^- of the samples were calculated from the isotopic conversion standard curve of N_2O and NO_3^-. The measurement accuracy of nitrogen is 0.08‰, and the measurement accuracy of oxygen is 0.24‰. The international standard USGS32 ($\delta^{15}N$ = +180‰, $\delta^{18}O$ = +25.7‰), USGS34 ($\delta^{15}N$ = -1.8‰, $\delta^{18}O$ = -27.9‰) and USGS35 (δ ^{15}N = +2.7‰, $\delta^{18}O$ = +57.5‰) with known isotope values were used. The $\delta^{15}N$ and $\delta^{18}O$ isotope are expressed as:

$$\delta^{15}N=[(^{15}N/^{14}N)_{sample}/(^{15}N/^{14}N)_{air} -1] \times 1000‰$$

$$\delta^{18}O=[(^{18}O/^{16}O)_{sample}/(^{18}O/^{16}O)_{SMOW} -1] \times 1000‰$$

Where $(^{15}N/^{14}N)_{air}$ represents the $\delta^{15}N$ of atmospheric N_2 in air and $(^{18}O/^{16}O)_{SMOW}$ is the ^{18}O of Vienna Standard Mean Ocean water.

2.4 Air mass trajectory analysis

The backward trajectory is the analysis of the source and transmission path of the air mass based on the path of the atmospheric air mass moving in a certain period of time. The GDAS data provided by the US Air Quality Laboratory (NOAA ARL) is used. TrajStat was used to calculate the 48h air mass backward trajectory during the sampling. The trajectory calculation module of HYSPLIT was included in TrajStat as an external process to calculate trajectories (Wang et al., 2009). For every month, the

daily 24h backward trajectory was calculated, with the set of 500m above sea level. We also do the cluster analysis for seasons. The number of cluster is three among all the seasons.

3 Results

3.1 Characteristics of $PM_{2.5}$, NO_3^- and WSIs

The concentration of $PM_{2.5}$ ranged from 11 to 198 $\mu g.m^{-3}$, with an average $PM_{2.5}$ of 50.6±33.9 $\mu g/m^3$ (Table S1), higher than the NAAQS Grade I (35 $\mu g.m^{-3}$). The highest $PM_{2.5}$ is 198$\mu g.m^{-3}$, in autumn. According to different seasons, the concentration of $PM_{2.5}$ was significant higher in autumn (82.7±43.6 $\mu g.m^{-3}$) than in winter (49.3±17.3 $\mu g.m^{-3}$), spring (40.7±18.0 $\mu g.m^{-3}$) and summer (23.0±8.7 $\mu g.m^{-3}$). The increase in concentration of $PM_{2.5}$ was accompanied by an increase in the concentration of WSIs (Figure 1). The average concentration of WSIs in $PM_{2.5}$ was 18.1±10.4 $\mu g.m^{-3}$, which behaved as higher in autumn and spring than in winter and summer (Table S1). WSIs accounted for 38.9% of $PM_{2.5}$ annually, and it was similar to the ratio in Suzhou (40%), lower than that in Beijing (51.5%) and higher than that in Shanghai (32%) (Tian et al., 2016; Gao et al., 2018; Qiao et al., 2015). Mean concentration of NO_3^- in $PM_{2.5}$ was 4.2±3.2 $\mu g.m^{-3}$ with the highest in autumn (6.2±4.1 $\mu g.m^{-3}$) and lowest in summer (2.1±1.0 $\mu g.m^{-3}$). As shown in Figure 1, $PM_{2.5}$, WSIs and NO_3^- had the same tendency at the same time, with the highest in autumn among all the seasons, indicating that autumn was the most polluted season and NO_3^- may dominant the pollution. Usually $PM_{2.5}$ is highest in winter and lowest in summer (Song et al., 2019), which is different from this study. Cao et al. (Cao et al., 2017)

found that the concentration of atmospheric $PM_{2.5}$ in Northeast China is much higher during biomass burning (261±163μg.m^{-3}) than during non-biomass burning (31.7±17.3 μg.m^{-3}). Due to the serious biomass burning in autumn in Northeast China, it may lead to the highest concentration of $PM_{2.5}$ in autumn of our study.

As is shown in Figure 1, the concentration of nitrate increased significantly with increasing concentration of $PM_{2.5}$, which was consistent with the observations in eastern China (Bao et al., 2019) and Beijing (Huang et al., 2016). According to the analysis of the proportion of ionic components, the annual nitrate accounted for the highest proportion (21.1%) compared with other ions (Figure 2a). Besides, the concentration of nitrate increased sharply during periods of severe pollution ($PM_{2.5}$≥75 μg.m^{-3}), as shown in Figure 2b. This indicates that it is necessary to urgently control the concentration of nitrate and study its source to provide a basis for solving air pollution in the Northeast region.

The correlation analysis between some major ionic components during the whole sampling was performed in Figure S3. NO_3^- had strong correlation with Cl^-, Mg^{2+}, Ca^{2+} and K^+, respectively ($p<0.01$), indicating that they had similar sources. There was a very high contribution of Cl^-, especially in autumn and winter (Figure 2a). Cl^- is derived from biomass burning (Zhang et al., 2018) and coal combustion (Hong et al., 2018). A high fraction of Ca^{2+} was also observed, especially in spring (Figure 2a). Ca^{2+} can be used as a tracer for crust source (Huang et al., 2018). In spring Ca^{2+} was as high as 13.5% and as we all known that dust is most common in spring. The prevailing winds in the area are northwest, and there are multi-desert and saline-alkali

land in the Northwest Jilin Province, therefore the annual Ca^{2+} was higher. Mg^{2+} can be derived from soil dust sources (Hong et al., 2018; Shao et al., 2018). Mg^{2+} and Ca^{2+} were well correlated throughout the year ($p<0.01$, Figure S3), so they may have similar sources. These two ions also have a good correlation with nitrate, therefore the soil source of nitrate cannot be ignored. K^+ is mainly emitted from coal combustion and biomass burning (Shao et al., 2018). The proportion of K^+ increased in autumn and winter, which indicated that the combustion source of autumn and winter contributes a lot. The higher content of SO_4^{2-}, Cl^- and K^+ are all related to the combustion source, thus the combustion source may be the main pollution source of nitrate in this area.

3.2 Seasonal characteristic of $\delta^{15}N\text{-}NO_3^-$ and $\delta^{18}O\text{-}NO_3^-$

The $\delta^{15}N\text{-}NO_3^-$ of $PM_{2.5}$ during sampling ranged from -2.70‰ to +20.01‰, with an annual mean of +7.18‰±5.12‰ (Table S1). This is similar to Beijing (Luo et al., 2019; Song et al., 2019) and BH island (Zong et al., 2017) in China. $\delta^{15}N\text{-}NO_3^-$ behaved great seasonal variation, especially higher in winter (13.79‰±2.17‰) than in summer (2.69‰±2.95‰) (Figure 3), which was the same with other researches (Beyn et al., 2014; Wankel et al., 2010; Xing and Liu, 2012). This may indicate differences in contributions from different sources. In winter, the increase in ^{15}N-rich NO_X from combustion sources may lead to higher $\delta^{15}N\text{-}NO_3^-$, and in summer, the increase in NO emissions from natural sources may lead to lower $\delta^{15}N\text{-}NO_3^-$ (Elliott et al., 2019; Fang et al., 2011; He et al., 2018). Therefore, soil source may account for a high proportion in summer than other seasons due to the negative isotope value. And

all the isotope values were positive in winter (Figure 3), indicating that the combustion source contributed more in winter.

The $\delta^{18}O\text{-}NO_3^-$ ranged from +49.29‰ to +89.53‰, with the mean value of 68.16‰±9.52‰ (Table S1). It also performed as high values in winter (70.50‰±10.02‰) and low values (58.67‰±4.53‰) in summer (Figure 3), which had the same tendency of $\delta^{15}N\text{-}NO_3^-$. This seasonal variation of $\delta^{18}O\text{-}NO_3^-$ is mainly affected by the oxidation pathway, which is mainly caused by the amount of solar radiation (Wankel et al., 2010).

4 Discussion

4.1 Formation mechanisms of nitrate

4.1.1 Formation pathways of nitrate

$\delta^{18}O\text{-}NO_3^-$ contributes to the identification of the conversion pathway from NO_X to NO_3^- (Rose et al., 2019; Wankel et al., 2010). As is shown in Text S2, we used Zong et al. 's method (Zong et al., 2017) which using the Bayesian mixed model to estimate the proportion of OH· pathway and N_2O_5 pathway and to estimate $\delta^{15}N$-fractionation values during the transfer of NO_X to NO_3^-. Monte Carlo simulation was used. It is generally considered that two-thirds of the oxygen atoms in NO_3^- were derived from O_3 and one-third from OH· in the OH· generation pathway (R3, Text S1). The estimated average contribution changes of the OH· pathway are shown in the Figure 4 (summer: 79.4±6.1%, autumn: 55.6±20.5%, winter: 56.8±19.2%, and spring: 56.3± 14.6%). OH· pathway accounted for a relatively high proportion in all seasons,

284 especially 79.4±6.1% in summer. This may due to the high temperature in summer
285 and the high concentration of O_3 (Figure S4), which is conducive to gas phase
286 reaction (Wang et al., 2017). This indicated that atmospheric nitrate in the Northeast
287 China was mainly produced by the OH· reaction with NO_2. It is the same with a
288 regional background site in North China (Zong et al., 2017) but is different from the
289 relatively high proportion of the N_2O_5 heterogeneous hydrolysis pathway observed in
290 Beijing (Wang et al., 2017; Wang et al., 2018). This also explained the seasonal
291 characteristics of $\delta^{18}O\text{-}NO_3^-$. The $\delta^{18}O\text{-}NO_3^-$ generated in the OH· reaction is
292 relatively lower , therefore, the $\delta^{18}O\text{-}NO_3^-$ is relatively lower in summer due to the
293 high proportion of OH· pathway.

294 However, the differences in the proportion of OH· pathway in spring, autumn
295 and winter were not obviously (Figure 4). From the oxygen isotope values, it can be
296 seen in Table S1 that the ranges of $\delta^{18}O\text{-}NO_3^-$ in spring (70.66‰±6.51‰), autumn
297 (70.59‰±10.1‰) and winter (70.50‰±10.02‰) were relatively consistent. It is
298 worth noting that there were some particularly low fractions of OH· pathway in spring,
299 autumn and winter (Figure S5). This was found to be related to the concentration of
300 $PM_{2.5}$. The contribution of OH· pathway was significantly negatively correlated
301 ($r=-0.42$, $p<0.01$) with $PM_{2.5}$ concentration. When the contribution of OH· pathway
302 was lower than 40%, the average concentration of $PM_{2.5}$ was 77.4 $\mu g.m^{-3}$. This
303 phenomenon was particularly serious in autumn when the number of pollution days
304 ($PM_{2.5}\geq 75$ $\mu g.m^{-3}$) accounted for 40%. This may be due to the fact that when air
305 pollution is serious, the solar radiation is not obvious, thus the photochemical reaction

306 produces less OH radicals (He et al., 2018). It is not beneficial to the gas phase
307 oxidation reaction when the pollution is serious and when the solar radiation is low
308 (Wen et al., 2018a). This can also explain why the proportion of OH· pathway in
309 winter was not much lower than that in spring and autumn. In theory, the solar
310 radiation in winter is the weakest, and it should show a lower proportion of OH·
311 pathway than other seasons. Because of the more pollution incidents in the spring and
312 autumn of the region, it seemed that the proportion of OH· pathway of nitrate in
313 spring and autumn was not much higher than that in winter.

314 ***4.1.2 Nitrogen oxidation ratio***

315 NOR indicates the degree of oxidation of atmospheric NO_2 to nitrate, and it can
316 be expressed as $nNO_3^-/(nNO_3^-+nNO_2)$, where n is the molar concentration (Zhang et
317 al., 2018). During the whole sampling, the concentration of NO_3^- and NOR showed
318 the same changing trend, with the higher in autumn and spring than in summer and
319 winter (Figure S4), indicating that autumn and spring was more quickly to the
320 conversion of NO_2 to nitrate. Studies have shown that high humidity conditions are
321 conducive to the formation of nitrates (Wen et al., 2018a) and usually NOR and RH
322 have significant positive correlation. The Figure 5 shows the changes of NOR with
323 different O_3 concentration, temperature and humidity conditions. Interestingly, as
324 shown in Figure 5c, NOR did not increase with increasing relative humidity, instead it
325 had the opposite trend. Previous report has shown that gas-phase reactions are
326 positively related to temperature, while aqueous reactions are related to RH (Tian et
327 al., 2019). Actually, there is a negative correlation between NOR and RH throughout

the sampling process ($r=-0.32$, $p<0.05$), indicating that the aqueous phase may not be good for the formation of NO_3^-. As mentioned above, the OH· pathway in this area may be the main pathway for nitrate formation (Figure 4). Besides, higher O_3 concentration may indicate a stronger photochemical reaction and O_3 is a supplier of OH· during the day (Wen et al., 2018a). It was found that NOR showed better O_3 concentration dependence ($r=0.23$, $p<0.05$), and NOR increased significantly especially when the concentration of O_3 was above 200μg.m^{-3} (Figure 5a). Studies have shown that relatively lower temperature is beneficial to the gas-particle conversion process from NO_2 to nitrate (Fan et al., 2019; Zhao et al., 2016), however, when the temperature was between -10°C and 0°C, the average NOR was the highest (Figure 5b), indicating that the relative lower temperature was favorable for the formation of nitrate aerosol in this area. However, if the temperature is too low, it is not conducive to the formation of NO_2 to nitrate. The average NOR was lower than 0.05 when the temperature was lower than -10 °C (Figure 5b).

4.2 Sources of nitrate from the SIAR model

In this study, two cases were analyzed for NO_X sources, one was for four seasons the other was for heating or non-heating periods. It is generally considered in China that spring, summer, autumn and winter are March to May, June to August, September to November, and December to February, respectively. The heating period in the area is from October 25, 2017 to April 10, 2018, and the rest of the time is the non-heating period. According to the corrected $\delta^{15}N\text{-}NO_X$ value (after isotope fractionation correction, Table S1, Figure 3), this study used the method (Text S3) of Zong et al.

(Zong et al., 2017) and Chang et al. (Chang et al., 2018) to quantify the contribution of each source. In this work, the main contributors to NO_X were considered to be motor vehicle emissions (-3.71‰ ± 10.40‰) (Felix and Elliott, 2014; Spiro and Robertson, 1997; Walters et al., 2015a; Walters et al., 2015b), coal combustion (13.72‰±4.57‰) (Felix et al., 2015; Felix et al., 2012; Walters et al., 2015b), biological soils (-33.77‰±12.16‰) (Felix and Elliott, 2014; Li and Wang, 2008), and biomass burning (1.04‰±4.13‰) (Fibiger and Hastings, 2016). Here, the Bayesian isotope mixing model named as SIAR (Stable Isotope Analysis in R) was used to quantify multiple potential sources of NO_X, which assumed that the $\delta^{15}N$ value of gas nitric acid was similar to the nitrate in $PM_{2.5}$.

The SIAR results (Figure 6) showed that the contributions of NO_X from biomass burning, biological soil, traffic and coal combustion were different among different stages. The distinction between heating and non-heating periods was more visible than the four seasons. Contribution of coal combustion during heating period (46.9%±10.5%) was significantly higher than that of non-heating period (24.7%±8.0%), which can also be seen from the significantly higher $\delta^{15}N$ in the heating period (10.86‰±4.71‰) than in the non-heating period (4.04‰±2.89‰) (Table S1, Figure 1). This indicated a significant increase in coal combustion in the region during the heating season. It was shown that in the non-heating period, biomass burning was the dominant source of NO_X, which contributed 39.0%±11.5%, higher than the 27.5%±16.5% of heating period. From the perspective of seasonal changes, the differences in contributions of NO_X from spring and autumn were not

obvious. The contributions of biomass burning, soil, traffic and coal were 37.5%±12.0%, 13.0%±4.1%, 20.4%±9.1% and 29.1%±8.3%, respectively in spring; And were 35.3%±13.0%, 12.0%±4.6%, 21.8%±10.2% and 30.9%±9.2%, respectively in autumn. However, the contributions of coal, traffic and soil sources were significantly different in summer and winter. The traffic source contributed the highest in summer (22.7%±8.0%) and the lowest in winter (8.6%±5.2%), which was the same with the contribution of soil. It was 17.8%±3.7% in summer, significantly higher than the 2.9%±1.9% in winter. Researches show that NO_X emitted by biological soil is higher in warm season than in the cold season (Parton et al., 2001; Van Der A et al., 2006), especially in summer with the maximum amount of NO_X emissions. The soil in the northeast is fertile and there is a lot of farmland, which explains why soil sources in summer contributed up to 18%. Besides, the contribution of coal combustion was 51.5%±5.3% in winter and 21.5%±7.9% in summer. The high coal combustion contribution in winter was consistent with the significant correlation between sulfate and nitrate ($p<0.01$) and the high concentration of SO_2 (Figure S2b). The sudden increase in SO_2 emissions in winter indicated that a large amount of SO_2 was emitted from coal combustion in the region in winter. Clearly, the contribution of biomass burning was higher than 35% among four seasons. MODIS satellite fire points (Figure S6) indicated that there were many biomass burning in the area and the dominant wind up wind direction areas in spring, summer and autumn, therefore the proportion of biomass burning was also higher in those three seasons. However, there was no fire point in the sampling area in winter except for transmissions from the southwest

394 (Figure S6). But there are still agricultural wastes such as wood and crop waste used
395 in rural heating in Northeast China. Therefore, the contribution of biomass burning
396 cannot be ignored in winter. In fact, the haze days and the clean days were also
397 distinguished from the source analysis, but the results showed no significant
398 difference, indicating that the contribution of nitrate source in this area was not
399 affected by concentration of $PM_{2.5}$ (Figure S7). This is consistent with the findings of
400 Song et al. in Beijing (Song et al., 2019).

401 **Summary**

402 Autumn was the most polluted season of Northeast China, in which season the
403 concentration of $PM_{2.5}$, water-soluble ions and nitrates were the highest compared to
404 the other seasons. Obviously, the nitrate pollution in Northeast China was serious
405 because nitrate accounted for the highest proportion of water-soluble ions during the
406 sampling period. Identifying NO_X sources is important for controlling $PM_{2.5}$ of this
407 area. $\delta^{15}N\text{-}NO_3^-$ ranged from -2.7‰ to +20.1‰, and $\delta^{18}O\text{-}NO_3^-$ ranged from +49.3‰
408 to +89.5‰. Both $\delta^{15}N\text{-}NO_3^-$ and $\delta^{18}O\text{-}NO_3^-$ were higher in winter than in summer,
409 which revealing the difference in sources and contributions from the nitrate formation
410 pathway among seasons. Besides, the isotope value in heating period was
411 significantly higher than in the non-heating period. The main formation pathway of
412 atmospheric nitrate in Northeast China was gas phase reaction of OH·, especially in
413 summer. The SIAR source analysis results showed that the source of NO_X in
414 Northeast China was dominated by coal combustion and the biomass burning,
415 followed by traffic emissions and soil emissions. During heating period, coal

combustion was the main source of NO_X (46.9%). A significant increase in SO_2 concentration during the heating phase indicated the significant increase in coal combustion during heating period. However, during non-heating period, biomass burning dominated (39.5%), which showed severe biomass burning phenomenon in the area. From seasonal perspective, the dominant source of NO_X in winter was coal combustion, while other seasons was biomass burning. Therefore, controlling coal combustion and biomass burning plays a leading role in reducing nitrate concentrations in Northeast China.

Disclosure statement

No potential conflict of interest was reported by the authors.

CRediT authorship contributions statement

Fang Cao: Project investigator, Methodological guidance.

Zhu-Yu Zhao: Writing-Original Draft, Data Curation.

Mei-Yi Fan: Data acquisition and analysis.

Wen-Qi Zhang, Xiao-Yao Zhai: Data acquisition.

Qian Wang: Chemical analysis.

Yan-Lin Zhang: Writing- Review & Editing, Method design.

Acknowledgements

This study was financially supported by the National Key R&D Program of China (Nos.2017YFC0212302 and Nos. 2017YFC0212704), National Nature Science Foundation of China (No. 41977305 and No. 41977185), the Provincial Natural Science Foundation of Jiangsu (No. BK20180040), Jiangsu Innovation & Entrepreneurship Team.

References

Anenberg, S.C., Miller, J., Minjares, R., Du, L., Henze, D.K., Lacey, F., Malley, C.S., Emberson, L., Franco, V., Klimont, Z., Heyes, C., 2017. Impacts and mitigation of excess diesel-related NOx emissions in 11 major vehicle markets. Nature 545, 467-471.

Bao, Z., Chen, L., Li, K., Han, L., Wu, X., Gao, X., Azzi, M., Cen, K., 2019. Meteorological and chemical impacts on $PM_{2.5}$ during a haze episode in a heavily polluted basin city of eastern China. Environ Pollut 250, 520-529.

Beyn, F., Matthias, V., Dahnke, K., 2014. Changes in atmospheric nitrate deposition in Germany--an isotopic perspective. Environ Pollut 194, 1-10.

Boningari, T., Smirniotis, P.G., 2016. Impact of nitrogen oxides on the environment and human health: Mn-based materials for the NOx abatement. Curr. Opin. Chem. Eng 13, 133-141.

Cao, F., Zhang, S.-C., Kawamura, K., Liu, X., Yang, C., Xu, Z., Fan, M., Zhang, W., Bao, M., Chang, Y., Song, W., Liu, S., Lee, X., Li, J., Zhang, G., Zhang, Y.-L., 2017. Chemical characteristics of dicarboxylic acids and related organic compounds in $PM_{2.5}$ during biomass-burning and non-biomass-burning seasons at a rural site of Northeast China. Environ Pollut 231, 654-662.

Chai, J.J., Miller, D.J., Scheuer, E., Dibb, J., Selimovic, V., Yokelson, R., Zarzana, K.J., Brown, S.S., Koss, A.R., Warneke, C., Hastings, M., 2019. Isotopic characterization of nitrogen oxides (NOx), nitrous acid (HONO), and nitrate (pNO_3^-) from laboratory biomass burning during FIREX. Atmospheric Measurement Techniques 12, 6303-6317.

Chang, Y., Zhang, Y., Tian, C., Zhang, S., Ma, X., Cao, F., Liu, X., Zhang, W., Kuhn, T., Lehmann, M.F., 2018. Nitrogen isotope fractionation during gas-to-particle conversion of NOx to NO_3^- in the atmosphere–implications for isotope-based NOx source apportionment. Atmos. Chem. Phys 18, 11647-11661.

Chen, D., Liu, Z., Fast, J., Ban, J., 2016. Simulations of sulfate–nitrate–ammonium (SNA) aerosols during the extreme haze events over northern China in October 2014. Atmos. Chem. Phys 16, 10707-10724.

Chen, F., Lao, Q., Jia, G., Chen, C., Zhu, Q., Zhou, X., 2019. Seasonal variations of nitrate dual isotopes in wet deposition in a tropical city in China. Atmos Environ 196, 1-9.

Elliott, E.M., Kendall, C., Wankel, S.D., Burns, D.A., Boyer, E.W., Harlin, K., Bain, D.J., Butler, T.J., 2007. Nitrogen Isotopes as Indicators of NOx Source Contributions to Atmospheric Nitrate Deposition Across the Midwestern and Northeastern United States. Environ Sci Technol 41, 7661-7667.

Elliott, E.M., Yu, Z., Cole, A.S., Coughlin, J.G., 2019. Isotopic advances in understanding reactive nitrogen deposition and atmospheric processing. Sci Total Environ 662, 393-403.

Fan, M.-Y., Zhang, Y.-L., Lin, Y.-C., Chang, Y.-H., Cao, F., Zhang, W.-Q., Hu, Y.-B., Bao, M.-Y., Liu, X.-Y., Zhai, X.-Y., Lin, X., Zhao, Z.-Y., Song, W.-H., 2019. Isotope-based source apportionment of nitrogen-containing aerosols: A case study in an industrial city in China. Atmos Environ 212, 96-105.

Fang, Y.T., Koba, K., Wang, X.M., Wen, D.Z., Li, J., Takebayashi, Y., Liu, X.Y., Yoh, M., 2011. Anthropogenic imprints on nitrogen and oxygen isotopic composition of precipitation nitrate in a nitrogen-polluted city in southern China. Atmos. Chem. Phys 11, 1313-1325.

Felix, J.D., Elliott, E.M., 2014. Isotopic composition of passively collected nitrogen dioxide emissions: Vehicle, soil and livestock source signatures. Atmos Environ 92, 359-366.

Felix, J.D., Elliott, E.M., Avery, G.B., Kieber, R.J., Mead, R.N., Willey, J.D., Mullaugh, K.M., 2015. Isotopic composition of nitrate in sequential Hurricane Irene precipitation samples: Implications for changing NOx sources. Atmos Environ 106, 191-195.

Felix, J.D., Elliott, E.M., Shaw, S.L., 2012. Nitrogen isotopic composition of coal-fired power plant NOx: influence of emission controls and implications for global emission inventories. Environ Sci Technol 46, 3528-3535.

Feng, T., Bei, N., Zhao, S., Wu, J., Li, X., Zhang, T., Cao, J., Zhou, W., Li, G., 2018. Wintertime nitrate formation during haze days in the Guanzhong basin, China: A case study. Environ Pollut 243, 1057-1067.

Fibiger, D.L., Hastings, M.G., 2016. First Measurements of the Nitrogen Isotopic Composition of NOx from Biomass Burning. Environ Sci Technol 50, 11569-11574.

Gao, H., Wei, J., Wang, Y., 2018. Seasonal variation and source analysis of water-soluble inorganic salts in PM2. 5 in the southern suburbs of Beijing. Huan jing ke xue= Huanjing kexue 39, 1987-1993.

Gu, D., Wang, Y., Smeltzer, C., Liu, Z., 2013. Reduction in NOx Emission Trends over China:

Regional and Seasonal Variations. Environ Sci Technol 47, 12912-12919.

Hastings, M.G., 2004. Seasonal variations in N and O isotopes of nitrate in snow at Summit, Greenland: Implications for the study of nitrate in snow and ice cores. J Geophys Res 109.

Hastings, M.G., Casciotti, K.L., Elliott, E.M., 2013. Stable Isotopes as Tracers of Anthropogenic Nitrogen Sources, Deposition, and Impacts. Elements 9, 339-344.

He, P., Xie, Z., Chi, X., Yu, X., Fan, S., Kang, H., Liu, C., Zhan, H., 2018. Atmospheric $\Delta^{17}O(NO_3^-)$ reveals nocturnal chemistry dominates nitrate production in Beijing haze. Atmos. Chem. Phys 18, 14465-14476.

Hong, Y., Li, C., Li, X., Ma, Y., Zhang, Y., Zhou, D., Wang, Y., Liu, N., Chang, X., 2018. Analysis of Compositional Variation and Source Characteristics of Water-Soluble Ions in $PM_{2.5}$ during Several Winter-Haze Pollution Episodes in Shenyang, China. Atmosphere 9, 280.

Hong, Y., Ma, Y., Sun, J., Li, C., Zhang, Y., Li, X., Zhou, D., Wang, Y., Liu, N., 2019. Water-soluble ion components of PM_{10} during the winter-spring season in a typical polluted city in Northeast China. Environ Sci Pollut R 26, 7055-7070.

Huang, X., Liu, Z., Zhang, J., Wen, T., Ji, D., Wang, Y., 2016. Seasonal variation and secondary formation of size-segregated aerosol water-soluble inorganic ions during pollution episodes in Beijing. Atmos Res 168, 70-79.

Huang, X., Zhang, J., Luo, B., Wang, L., Tang, G., Liu, Z., Song, H., Zhang, W., Yuan, L., Wang, Y., 2018. Water-soluble ions in $PM_{2.5}$ during spring haze and dust periods in Chengdu, China: Variations, nitrate formation and potential source areas. Environ Pollut 243, 1740-1749.

Itahashi, S., Yumimoto, K., Uno, I., Hayami, H., Fujita, S.I., Pan, Y., Wang, Y., 2018. A 15-year record (2001–2015) of the ratio of nitrate to non-sea-salt sulfate in precipitation over East Asia. Atmospheric Chemistry & Physics 18, 1-30.

Li, D., Wang, X., 2008. Nitrogen isotopic signature of soil-released nitric oxide (NO) after fertilizer application. Atmos Environ 42, 4747-4754.

Li, H., Zhang, Q., Zheng, B., Chen, C., Wu, N., Guo, H., Zhang, Y., Zheng, Y., Li, X., He, K., 2018. Nitrate-driven urban haze pollution during summertime over the North China Plain. Atmos. Chem. Phys 18, 5293-5306.

Li, N., Han, W., Wei, X., Shen, M., Sun, S., 2019. Chemical characteristics and human health assessment of PM_1 during the Chinese Spring Festival in Changchun, Northeast China.

Atmospheric Pollution Research 10, 1823-1831.

Luo, L., Wu, Y., Xiao, H., Zhang, R., Lin, H., Zhang, X., Kao, S.J., 2019. Origins of aerosol nitrate in Beijing during late winter through spring. Sci Total Environ 653, 776-782.

Ma, G., Zhao, T., Kong, S., Bao, Y., Chen, C., Gong, S., Guo, J., Yu, C., Wu, M., Chang, J., 2018. Variations in FINN Emissions of Particulate Matters and Associated Carbonaceous Aerosols from Remote Sensing of Open Biomass Burning over Northeast China during 2002–2016. Sustainability 10, 3353.

Parton, W., Holland, E., Del Grosso, S., Hartman, M., Martin, R., Mosier, A., Ojima, D., Schimel, D., 2001. Generalized model for NOx and N_2O emissions from soils. J. Geophys. Res.: Atmos 106, 17403-17419.

Pathak, R.K., Wu, W.S., Wang, T., 2009. Summertime $PM_{2.5}$ ionic species in four major cities of China: nitrate formation in an ammonia-deficient atmosphere. Atmos. Chem. Phys 9, 1711-1722.

Qiao, T., Zhao, M., Xiu, G., Yu, J., 2015. Seasonal variations of water soluble composition (WSOC, Hulis and WSIIs) in PM1 and its implications on haze pollution in urban Shanghai, China. Atmos Environ 123, 306-314.

Ren, X., Sun, R., Meng, X., Vorobiev, N., Schiemann, M., Levendis, Y.A., 2017. Carbon, sulfur and nitrogen oxide emissions from combustion of pulverized raw and torrefied biomass. Fuel 188, 310-323.

Rose, L.A., Yu, Z., Bain, D.J., Elliott, E.M., 2019. High resolution, extreme isotopic variability of precipitation nitrate. Atmos Environ 207, 63-74.

Shao, P., Tian, H., Sun, Y., Liu, H., Wu, B., Liu, S., Liu, X., Wu, Y., Liang, W., Wang, Y., Gao, J., Xue, Y., Bai, X., Liu, W., Lin, S., Hu, G., 2018. Characterizing remarkable changes of severe haze events and chemical compositions in multi-size airborne particles (PM_1, $PM_{2.5}$ and PM_{10}) from January 2013 to 2016–2017 winter in Beijing, China. Atmos Environ 189, 133-144.

Shi, X., Nenes, A., Xiao, Z., Song, S., Yu, H., Shi, G., Zhao, Q., Chen, K., Feng, Y., Russell, A.G., 2019. High-Resolution Data Sets Unravel the Effects of Sources and Meteorological Conditions on Nitrate and Its Gas-Particle Partitioning. Environ Sci Technol 53, 3048-3057.

Shi, Y., Xia, Y.-f., Lu, B.-h., Liu, N., Zhang, L., Li, S.-j., Li, W., 2014. Emission inventory and trends of NOx for China, 2000–2020. Journal of Zhejiang University Science A 15, 454-464.

Skalska, K., Miller, J.S., Ledakowicz, S., 2010. Trends in NOx abatement: a review. Sci Total Environ 408, 3976-3989.

Song, W., Wang, Y.L., Yang, W., Sun, X.C., Tong, Y.D., Wang, X.M., Liu, C.Q., Bai, Z.P., Liu, X.Y., 2019. Isotopic evaluation on relative contributions of major NOx sources to nitrate of $PM_{2.5}$ in Beijing. Environ Pollut 248, 183-190.

Spiro, B., Robertson, S.M.C., 1997. Potential canopy influences on the isotopic composition of nitrogen and sulphur in atmospheric deposition. Oecologia 109, 600-607.

Sun, Z., Duan, F., He, K., Du, J., Zhu, L., 2019. Sulfate-nitrate-ammonium as double salts in $PM_{2.5}$: Direct observations and implications for haze events. Sci Total Environ 647, 204-209.

Tian, M., Liu, Y., Yang, F., Zhang, L., Peng, C., Chen, Y., Shi, G., Wang, H., Luo, B., Jiang, C., Li, B., Takeda, N., Koizumi, K., 2019. Increasing importance of nitrate formation for heavy aerosol pollution in two megacities in Sichuan Basin, southwest China. Environ Pollut 250, 898-905.

Tian, M., Wang, H., Chen, Y., Yang, F., Zhang, X., Zou, Q., Zhang, R., Ma, Y., He, K., 2016. Characteristics of aerosol pollution during heavy haze events in Suzhou, China. Atmos. Chem. Phys 16, 7357-7371.

Van Der A, R., Peters, D., Eskes, H., Boersma, K., Van Roozendael, M., De Smedt, I., Kelder, H., 2006. Detection of the trend and seasonal variation in tropospheric NO_2 over China. J. Geophys. Res.: Atmos 111.

Walters, W.W., Goodwin, S.R., Michalski, G., 2015a. Nitrogen stable isotope composition ($\delta^{15}N$) of vehicle-emitted NOx. Environ Sci Technol 49, 2278-2285.

Walters, W.W., Michalski, G., 2016. Theoretical calculation of oxygen equilibrium isotope fractionation factors involving various NO molecules, OH, and H_2O and its implications for isotope variations in atmospheric nitrate. Geochim Cosmochim Ac 191, 89-101.

Walters, W.W., Tharp, B.D., Fang, H., Kozak, B.J., Michalski, G., 2015b. Nitrogen Isotope Composition of Thermally Produced NOx from Various Fossil-Fuel Combustion Sources. Environ Sci Technol 49, 11363-11371.

Wang, H., Lu, K., Chen, X., Zhu, Q., Chen, Q., Guo, S., Jiang, M., Li, X., Shang, D., Tan, Z., Wu, Y., Wu, Z., Zou, Q., Zheng, Y., Zeng, L., Zhu, T., Hu, M., Zhang, Y., 2017. High N_2O_5 Concentrations Observed in Urban Beijing: Implications of a Large Nitrate Formation

Pathway. Environmental Science & Technology Letters 4, 416-420.

Wang, H., Lu, K., Chen, X., Zhu, Q., Wu, Z., Wu, Y., Sun, K., 2018. Fast particulate nitrate formation via N_2O_5 uptake aloft in winter in Beijing. Atmos. Chem. Phys 18, 10483-10495.

Wang, Y., Zhang, X., Draxler, R.R., 2009. TrajStat: GIS-based software that uses various trajectory statistical analysis methods to identify potential sources from long-term air pollution measurement data. Environmental Modelling and Software 24, 938-939.

Wang, Y.L., Song, W., Yang, W., Sun, X.C., Tong, Y.D., Wang, X.M., Liu, C.Q., Bai, Z.P., Liu, X.Y., 2019. Influences of atmospheric pollution on the contributions of major oxidation pathways to $PM_{2.5}$ nitrate formation in Beijing. J. Geophys. Res.: Atmos 124, 4174-4185.

Wankel, S.D., Chen, Y., Kendall, C., Post, A.F., Paytan, A., 2010. Sources of aerosol nitrate to the Gulf of Aqaba: Evidence from $\delta^{15}N$ and $\delta^{18}O$ of nitrate and trace metal chemistry. Mar Chem 120, 90-99.

Wen, L., Xue, L., Wang, X., Xu, C., Chen, T., Yang, L., Wang, T., Zhang, Q., Wang, W., 2018a. Summertime fine particulate nitrate pollution in the North China Plain: increasing trends, formation mechanisms and implications for control policy. Atmos. Chem. Phys 18, 11261-11275.

Wen, X., Zhang, P., Liu, D., 2018b. Spatiotemporal Variations and Influencing Factors Analysis of $PM_{2.5}$ Concentrations in Jilin Province, Northeast China. Chinese geographical science 28, 810-822.

Xing, M., Liu, W., 2012. Variations in the concentration and isotopic composition of nitrate nitrogen in wet deposition and their relation with meteorological conditions in Xi'an city, Northwest China. Appl Geochem 27, 831-840.

Xu, Q., Wang, S., Jiang, J., Bhattarai, N., Li, X., Chang, X., Qiu, X., Zheng, M., Hua, Y., Hao, J., 2019. Nitrate dominates the chemical composition of $PM_{2.5}$ during haze event in Beijing, China. Sci Total Environ 689, 1293-1303.

Yang, T., Sun, Y., Zhang, W., Wang, Z., Liu, X., Fu, P., Wang, X., 2017. Evolutionary processes and sources of high-nitrate haze episodes over Beijing, Spring. Journal of Environmental Sciences 54, 142-151.

Yu, Z., Elliott, E.M., 2017. Novel Method for Nitrogen Isotopic Analysis of Soil-Emitted Nitric Oxide. Environ Sci Technol 51, 6268-6278.

618 Zhang, J., Liu, L., Wang, Y., Ren, Y., Wang, X., Shi, Z., Zhang, D., Che, H., Zhao, H., Liu, Y.,
619 2017. Chemical composition, source, and process of urban aerosols during winter haze
620 formation in Northeast China. Environ Pollut 231, 357-366.
621 Zhang, R., Sun, X., Shi, A., Huang, Y., Yan, J., Nie, T., Yan, X., Li, X., 2018. Secondary inorganic
622 aerosols formation during haze episodes at an urban site in Beijing, China. Atmos Environ
623 177, 275-282.
624 Zhang, Y.-L., Cao, F., 2015. Is it time to tackle $PM_{2.5}$ air pollutions in China from biomass-burning
625 emissions? Environ Pollut 202, 217-219.
626 Zhao, B., Wang, S.X., Liu, H., Xu, J.Y., Fu, K., Klimont, Z., Hao, J.M., He, K.B., Cofala, J.,
627 Amann, M., 2013. NOx emissions in China: historical trends and future perspectives. Atmos.
628 Chem. Phys 13, 9869-9897.
629 Zhao, M., Xiu, G., Qiao, T., Li, Y., Yu, J., 2016. Characteristics of Haze Pollution Episodes and
630 Analysis of a Typical Winter Haze Process in Shanghai. Aerosol and Air Quality Research 16,
631 1625-1637.
632 Zhao, Z.-Y., Cao, F., Zhang, W.-Q., Zhai, X.-Y., Fang, Y., Fan, M.-Y., Zhang, Y.-L., 2019.
633 Determination of Stable Nitrogen and Oxygen Isotope Ratios in Atmospheric Aerosol
634 Nitrates. Chinese J Anal Chem 47, 907-915.
635 Zong, Z., Tan, Y., Wang, X., Tian, C., Fang, Y., Chen, Y., Fang, Y., Han, G., Li, J., Zhang, G., 2018.
636 Assessment and quantification of NOx sources at a regional background site in North China:
637 Comparative results from a Bayesian isotopic mixing model and a positive matrix
638 factorization model. Environ Pollut 242, 1379-1386.
639 Zong, Z., Wang, X., Tian, C., Chen, Y., Fang, Y., Zhang, F., Li, C., Sun, J., Li, J., Zhang, G., 2017.
640 First Assessment of NOx Sources at a Regional Background Site in North China Using
641 Isotopic Analysis Linked with Modeling. Environ Sci Technol 51, 5923-5931.
642

643 **Figure Captions**

644 Fig. 1 Time series of $PM_{2.5}$, $\delta^{15}N$, NO_3^- and WSIs during sampling.

645 Fig. 2 The proportion of main inorganic ion component of $PM_{2.5}$ (a)during the whole

646 sampling and (b)during the clean days ($PM_{2.5}$<75 μg.m^{-3}) and haze days ($PM_{2.5}$≥75

647 μg.m^{-3}).

648 Fig. 3 Seasonal characteristics of $^{15}N\text{-}NO_3^-$ and $\delta^{18}O\text{-}NO_3^-$ in $PM_{2.5}$.

649 Fig. 4 The box plot of proportion of nitrate formed by the OH radical pathway.

650 Fig. 5 The box plot of NO_2, NO_3^-, NOR, T, RH and O_3 during the spring, summer,

651 autumn, winter, heating and non-heating period.

652 Fig. 6 Potential contribution of coal, traffic vehicle, biomass burning and biogenic soil

653 emission of NO_3^- in $PM_{2.5}$ during (a)spring, (b)summer, (c)autumn, (d)winter,

654 (e)heating and (f)non-heating period.

655

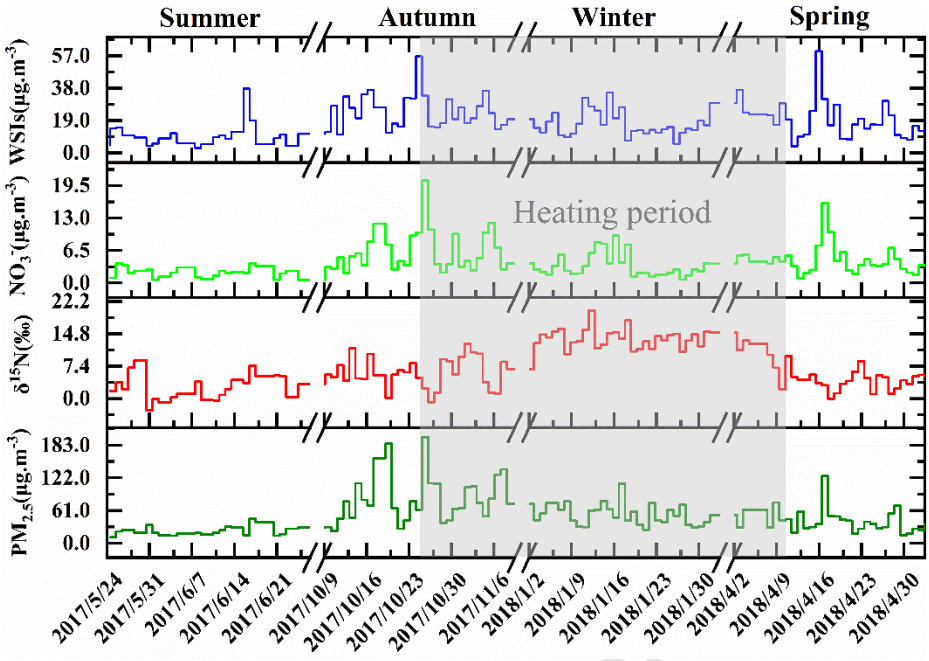

656

657 **Figure 1** Time series of $PM_{2.5}$, $\delta^{15}N$, NO_3^- and WSIs during sampling.

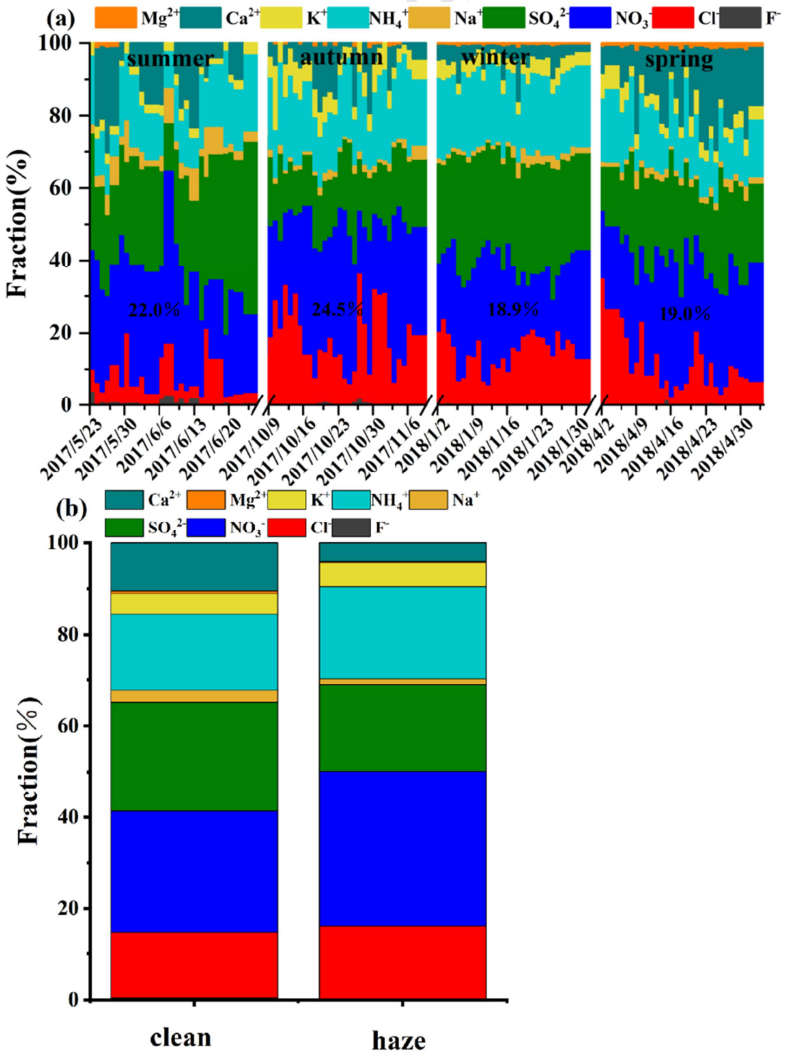

658

659 **Figure 2** The proportion of main inorganic ion component of $PM_{2.5}$ (a)during the

660 whole sampling and (b)during the clean days ($PM_{2.5}$<75 μg.m^{-3}) and haze days

661 ($PM_{2.5}$≥75 μg.m^{-3}).

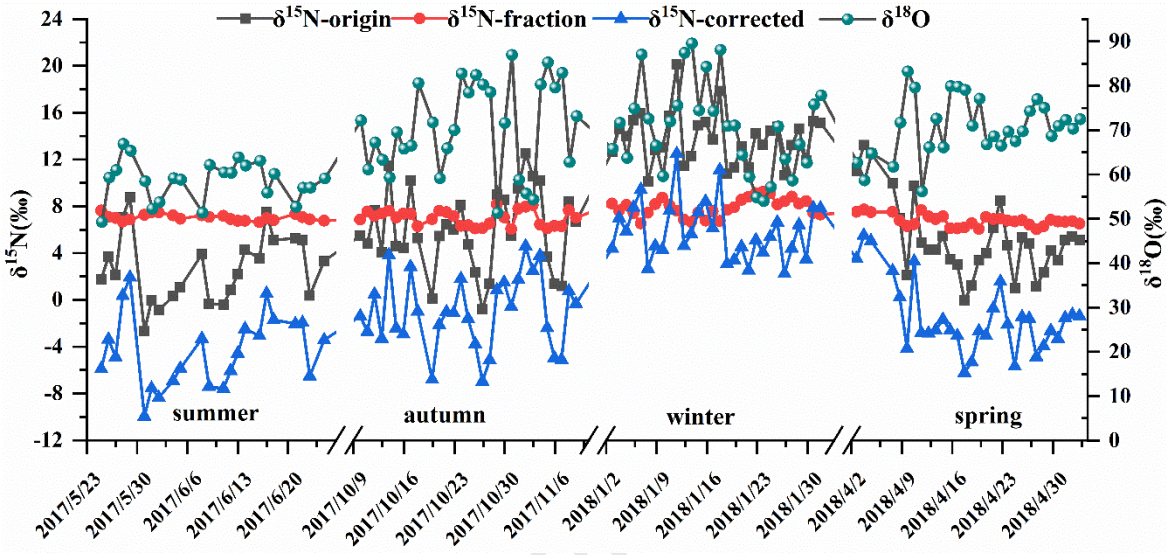

662 **Figure 3** Seasonal characteristics of $^{15}N\text{-}NO_3^-$ and $\delta^{18}O\text{-}NO_3^-$ in $PM_{2.5}$.

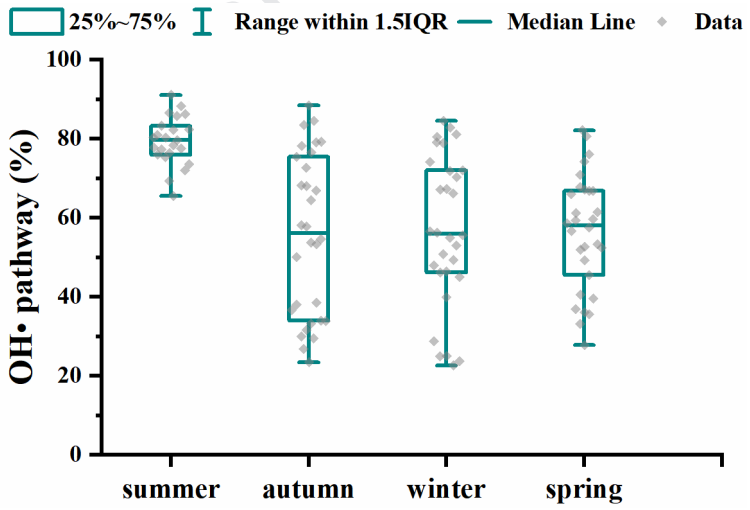

663

664 **Figure 4** The box plot of proportion of nitrate formed by the OH radical

665 pathway.

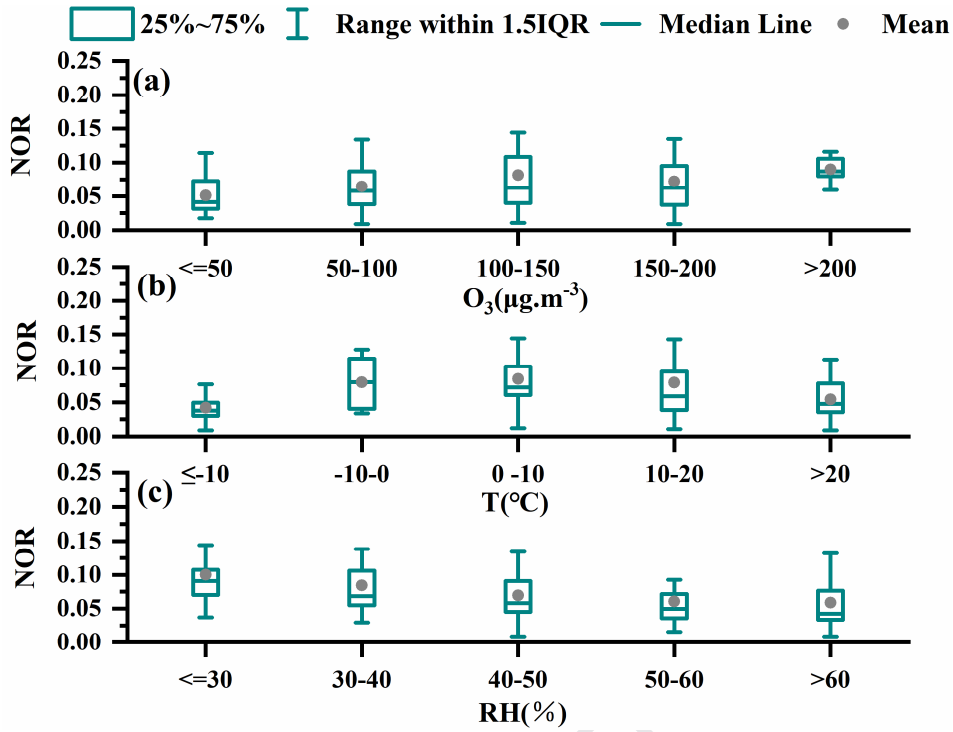

Figure 5 NOR changes under different (a)O_3, (b)temperature and (c)humidity.

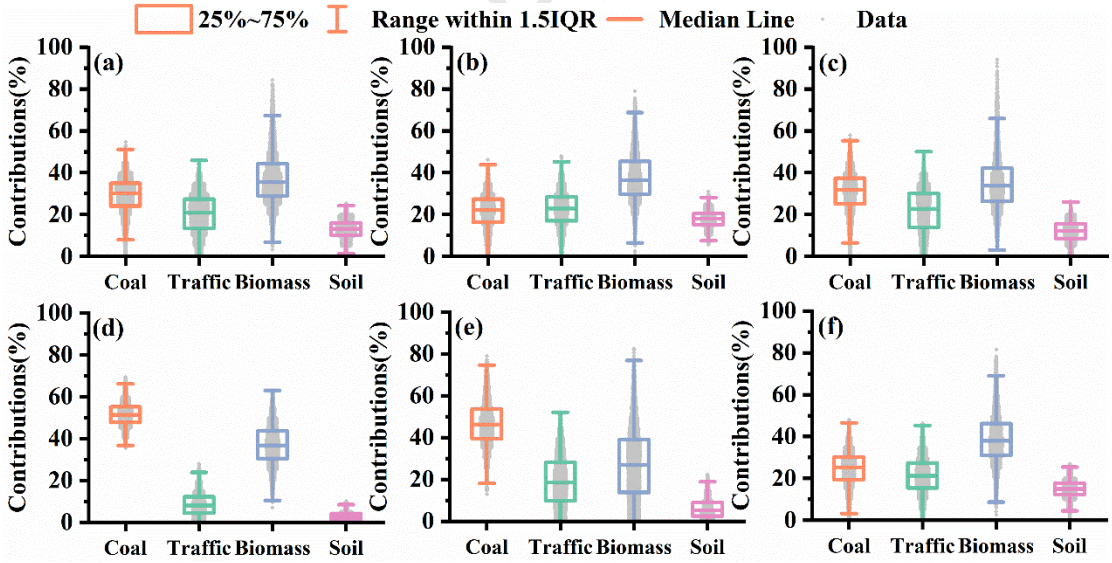

Figure 6 Potential contribution of coal, traffic vehicle, biomass burning and biogenic soil emission of NO_3^- in $PM_{2.5}$ during (a)spring, (b)summer, (c)autumn, (d)winter, (e)heating and (f)non-heating period.

Highlights:

Coal combustion and biomass burning dominated the production of nitrate in Northeast China.

Nitrate was formed mainly through the OH radical pathway in Northeast China.

The contribution of the sources varied significantly in different seasons, except for the largest contribution of coal combustion in winter, biomass burning contributed the most in other seasons.

The dominant source of nitrate during heating period and non-heating period were coal combustion and biomass burning, respectively.

Declaration of interests

☒ The authors declare that they have no known competing financial interests or personal relationships that could have appeared to influence the work reported in this paper.

☐The authors declare the following financial interests/personal relationships which may be considered as potential competing interests: